JMEPEG (2011) 20:1294–1303
DOI: 10.1007/s11665-010-9749-3

1059-9495/$19.00

Evaluation of the Low Heat Input Process for Weld Repair of Nickel-Base Superalloys

J. Durocher and N.L. Richards

(Submitted March 31, 2009; in revised form July 20, 2010)

The repair of turbine blades and vanes commonly involves gas tungsten arc welding or an equivalent process, but unfortunately these components are often susceptible to heat-affected zone (HAZ) cracking during the weld repair process. This is a major problem especially in cast alloys due to their coarse-grain size and where the (Al + Ti) contents is in excess of 3-4%; vacuum brazing is also used but mainly on low stress non-rotating components such as vanes. Micro-welding has the potential to deposit small amounts of filler at low heat input levels with minimum HAZ and thus is an attractive process for depositing a quality weld. As with conventional fusion processes, the filler alloy is deposited by the generation of a low power arc between a consumable electrode and the substrate. The low heat input of this process offers unique advantages over more common welding processes such as gas tungsten arc, plasma arc, laser, and electron beam welding. In this study, the low heat input characteristic of micro-welding has been used to simulate weld repair using Inconel (IN) (Inconel and IN are trademarks of INCO Alloys International) 625, Rene (Rene is a trademark of General Electric Company) 41, Nimonic (Nimonic is a trademark of INCO Alloys International) 105 and Inconel 738LC filler alloys, to a cast Inconel 738LC substrate. The effect of micro-welding process parameters on the deposition rate, coating quality, and substrate has been investigated.

Keywords aerospace, electron microscopy, joining, metallography, modeling processes, superalloys, welding

1. Introduction

In a previous article, we reported on the use of a low heat input welding process to repair alloy IN738 with filler metals containing up to about 3 wt.% (Al + Ti) and compared the joint properties with IN625 and IN738 fillers (Ref 1). In the present communication, we extend the (Al + Ti) filler levels up to nearly 6 wt.% using Rene 41 (Al + Ti = 4.7) and Nimonic 105 (Al + Ti = 5.9). Due to severe operating conditions in the gas turbine, cost effective repair schemes need to be economically viable for turbine users. Degradation occurs to components such as blades and vanes from factors such as alternating stresses, impurities in the fuel, operating temperature, water ingestion, and temperature cycling. These operating factors lead to component failure via mechanisms such as rupture, creep, high and low cycle fatigue, thermal fatigue, oxidation, erosion, corrosion, wear, and foreign object damage.

Maintenance schedules for turbines are predicated based on original equipment manufacturer's experience with their engines, and is an important economic consideration for operators. Thus, depending on a predetermined schedule, turbines are sent to repair centers for inspection, repair, and overhaul. Due to the varying stress levels along, for example, a turbine blade, restrictions occur as to the extent of repairs that can be made. With normally fusion type repairs using low strength weld fillers such as IN625, repairs tend to have reduced properties as compared to the base material and are often limited to the upper 10-20% portion of blades, where they experience the least amount of loading (Ref 2). Thus, present day welding processes fail to produce a repaired blade where the original properties have been fully restored. In the case where unacceptable damage is found outside the permitted repair area, blades must be replaced. Therefore, there is a significant economic impetus to the development of innovative repair techniques, processes, and the use of materials to increase the percentage of blades and other costly components that can be repaired.

One of the most commonly used turbine alloys is Inconel 738, being used on both aircraft and land-based turbines. The alloys is precipitation hardened by the γ' phase $Ni_3(Al, Ti)$ and also contains randomly dispersed MC type carbides. Unfortunately, due to its high strength and coarse-grain size, the cast alloy suffers from micro-fissuring in the weld heat-affected zone (HAZ) as a result of elemental segregation and/or grain boundary liquation during the weld cycle (Ref 3, 4). The micro-fissuring behavior is also exacerbated by a high (Al + Ti) content of over 6 wt.%, including liquation of the γ' phase (Ref 5). Thus, to reduce micro-fissuring in the HAZ, repair stations have traditionally resorted to the use of low strength fillers such as IN617 and IN625, these being low strength, solid solution type alloys with no perceptible precipitation hardening. Use of these low strength fillers therefore leads to inferior repair properties to the components in areas such as, wear, corrosion resistance, hardness, tensile strength, fatigue, and creep resistance (Ref 4).

Currently, the most prevalent repair methods used are gas tungsten arc welding (GTAW) and vacuum brazing techniques,

J. Durocher, Standard Aero Ltd., 33 Allen Dyne Road, Winnipeg, MB R3H 1A1, Canada; and **N.L. Richards**, Department of Mechanical and Manufacturing Engineering, University of Manitoba, Winnipeg, MB R2N 5V6, Canada. Contact e-mail: nrichar@cc.umanitoba.ca.

though other methods include: plasma transferred arc welding (PTAW), micro-plasma transferred arc welding, laser beam welding (LBW), diffusion brazing, wide gap diffusion brazing, and transient liquid phase bonding (Ref 6). The manual GTAW process is, however, the most common due to its relative low cost, simplicity and versatility, though the process is relatively slow, and that solid solution strengthened alloy fillers are required when welding high strength γ' precipitation hardenable alloys. Unfortunately, the use of high strength fillers leads to severe HAZ micro-fissuring especially when used in conjunction with fillers using (Al + Ti) levels over about 3 wt.% (Ref 4).

The alternative process of vacuum brazing is not permitted on highly stressed components such as blades, while diffusion type brazing processes are permitted for small crack repairs, limited to non-critical stationary components. The use of brazing type repair methods relies heavily on cleaning and removal of oxides from cracks for proper wetting and flow of the braze alloy. In addition, wide gap brazing techniques are available for re-building missing sections of airfoils, crack repair, and restoration of eroded wall thickness.

With the problems associated with present conventional techniques and the desire to use higher strength fillers alloys on high strength parent gas turbine alloys, cost effective, low heat input filler deposition processes offer potential alternatives. However, an understanding of the low heat input type processes is necessary to use these newer methods more effectively. In the present communication, we use one such process, where a consumable electrode is held in contact and deposited onto a conductive substrate using an arc with low pulse power levels. As with conventional arc processes, the resulting deposit is metallurgically bonded to the substrate. The repair of a gas turbine component is considered economical if the cost of the repair does not exceed approximately 40-60% (Ref 2) of the component's value. Therefore, the potential for a significant cost savings exists and may be achieved by low heat input material deposition processing such as micro-welding.

Many publications are available in the literature regarding low heat input applications to repair of components such as dies (Ref 7), oxidation resistance (Ref 8) and wear behavior (Ref 9) and also deposition characteristics (Ref 10, 11), though only limited microstructural studies on the repair of Ni-base superalloys (Ref 1, 12, 13). On cast Superalloy IN-792 Xie and Wang (Ref 12) showed that crack free deposits were possible on an alloy containing high levels of Ti and Al. While the layers are deposited in a sequential manner, grains grow in a preferred growth direction perpendicular to the deposit. X-ray diffraction showed the deposit, however, to be crystalline irrespective of the rapid cooling rate (Ref 12). Gregoi et al. (Ref 13) showed that using electro-spark deposition on single crystal alloy CSMX-10, that no cracking was present in the HAZ, unlike that shown by GTAW. While a previous article by the current authors (Ref 1) was more concerned with evaluating the effect of process parameters on the quality of the deposit, they also showed it was possible to deposit crack free layers, the process being viable for repair of high (Al + Ti) superalloys.

The present research program therefore was undertaken to evaluate the effect of micro-welding process parameters on the microstructural characteristics of Rene 41 and Nimonic 105, compared to electrodes made from IN 625 and IN 738 filler alloys and to model these effects. Statistical evaluations of the microstructural features of the deposit, relative to the processing values were also attempted, with a view to understand the process and optimize repairs of cast IN738 substrates.

2. Experimental Procedures

Electrode alloys were selected based on their (Al + Ti) content and relative to those used previously in Ref (1). In Ref (1), alloys used were Inconel 625 (Al + Ti $\leq$ 0.8), Inconel 718 (Al + Ti = 0.9), and Inconel 722 (Al + Ti = 2.4), and Inconel 738LC (Al + Ti = 6.8), all in wt.%. For the present communication, electrodes were selected as follows: IN625 (Al + Ti $\leq$ 0.8), Rene 41 (Al + Ti = 4.7), Nimonic 105 (Al + Ti = 5.9), and Inconel 738LC (Al + Ti = 6.80). Table 1 lists the chemical compositions of materials used in this study.

The base material was Inconel 738LC cast bar 6 mm thick by 25 mm wide by 175 mm long. To simulate several repair zones with a constant geometry, a rounded graphite electrode with a 9-mm diameter electrode with a radius of 16 mm was used to electrical-discharge machine (EDM) 0.6-mm deep hemispheres in the bars with a die sinker machine. The EDM's surface layers were subsequently removed by careful mechanical grinding with a carbide ball tool. Prior to applying weld deposits, the surface scale was removed by abrasive blasting with 180 grit aluminum oxide. Subsequently, the bars were sectioned to make individual specimens that were identified and weighed to the nearest 0.0001 g.

GTAW of baseline specimens was carried out using a CANOX C-SW300 AD/DC power supply. The welding process parameters were:

- Voltage: 10 ± 1 V
- Current: 20 ± 2 A
- Polarity: direct current, electrode negative
- Electrode: 2% thoriated tungsten
- Filler: Inconel 625 wire
- Cover gas: argon

Table 1 Chemical composition of materials (wt.%)

	IN738 (Notes 1 and 2)	IN625 (Note 3)	R41 (Note 3)	N105 (Note 3)
C	0.17	0.1 max	0.12 max	0.12 max
Co	8.5	1.0 max	11.0	20.0
Cr	16.0	21.5	20.0	14.8
Mo	1.7	9.0	9.75	5.0
W	2.6	0.0	0.0	0.0
Ta	1.7	-	0.0	0.0
Nb	0.9	3.65, w/Ta	0.0	0.0
Al	3.4	0.4 max	1.6	4.7
Ti	3.4	0.4 max	3.1	1.2
Al + Ti	6.8	0.8 max	4.7	5.9
B	0.01	0.0	0.007	0.006
Zr	0.05	0.0	0.0	0.15
Fe	0.5 max	5.0 max	5.0 max	1.0 max
Mn	0.2 max	0.5 max	0.0	1.0 max
Si	0.3 max	0.5 max	0.0	1.0 max
S	0.015 max	0.015 max	0.0	0.01 max
Ni	Balance	Balance	Balance	Balance
Cu	0.0	0.0	0.0	0.2 max
P	0.0	0.015 max	0.0	0.0
Pb	0.0	0.0	0.0	0.0015 max

Notes: 1. As-received composition. 2. Composition of substrate and electrode material. 3. Nominal compositions of electrode material

Table 2 Design of experiments

Specimen number	Capacitance, μF	Voltage, V	Current, A
1	20	100	3
2	50	100	3
3	20	200	3
4	50	200	3
5	20	100	5
6	50	100	5
7	20	200	5
8	50	200	5
9	30	150	4
10	30	150	4
11	30	150	4

The micro-welding equipment consists of a resistance-capacitance circuit, where the electrode is in brief contact with the substrate. In this study, Model PS98 MKII power supply with a manually operated AH98-MKIDD torch was used. To prevent fusion of the electrode to the substrate, it was rotated during the weld build-up process. Micro-welding process parameters that were controlled in this study were:

- Pulse duration: 25-50 μs
- Electrode rotational speed: 1100-1200 revolutions per minute
- Torch traverse speed: 6-12 mm per second
- Orientation: 30-45° from coated surface
- Contact force: approximately 1.0 N
- Cover gas: argon

The following micro-weld parameters were varied in the experiments: voltage, current, and capacitance. A two-level, three-factor with three center points design of experiments was devised for voltage, current, and capacitance using the following range of parameters: 100-200 V, 3-5 A, and 20-50 μF. Center points were included and repeated three times in the design of experiments in order to determine if curvature exists in the data. Since the pulse frequency depends on the selected parameters for voltage, current, and capacitance, it was treated as a floating variable and assumed not to have a direct effect on the results.

The responses investigated in this study were:

1. Deposition rate
2. Void content (volume fraction)
3. Crack density (total length/unit area)

For the micro-welding process each combination of voltage, current, and capacitance was carried out in accordance with the design of experiments listed in Table 2. The IN738 specimens were micro-weld coated in the as-received condition. Using each electrode material, the hemispheres were filled for a maximum period of 60 min or until a mound approximately 0.5 mm high protruded above the surrounding surface (in instances of high deposition rates).

The design of experiments for each response was analyzed using Minitab* statistical analysis software. p Values were obtained and assessed in order to quantify the effect of terms in the DOE. The p value for individual responses is a calculated term ranging from 0 to 1 which describes the probability that two populations have the same mean value. A high p value corresponds to a low probability that the population means are different and that a particular term does not have a significant effect on the response. It is common practice to use a threshold p value of 0.05 to draw conclusions but this can be overly restrictive in some cases. With a goal of establishing a general understanding of the micro-welding process, a threshold p value of 0.1 was selected in order to expand the process modeling results.

*Minitab is a trademark of Minitab Inc.

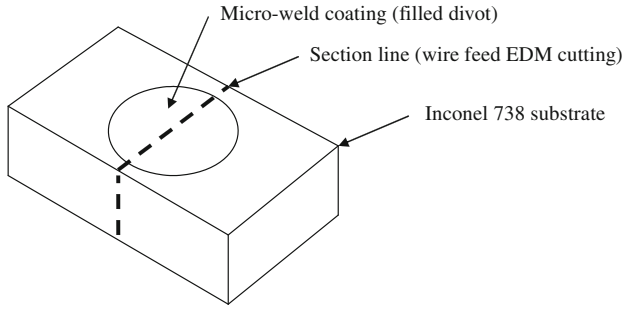

Fig. 1 Sketch showing sectioning of micro-welded-coated specimens

Welded specimens were sectioned using a wire feed EDM and subsequently processed using standard metallographic procedures. Figure 1 shows a diagram indicating the location of sections taken from micro-welded coated specimens. Kalling's no. 2 reagent was swabbed on the polished surface for 3-5 s followed by rinsing with cold distilled water in order to reveal the microstructure of the cast Inconel 738 base material and the micro-weld interface. This rendered the interface and weld microstructure visible but exaggerated the relative size of voids and cracks due to edge rounding. Therefore, all quantitative measurements were conducted in as-polished and unetched condition.

Using a Zeiss** microscope with Clemex† image analysis software, routines were established to measure the area fraction of voids and total crack length for selected field of view. Area fraction void content measurements were taken at a magnification of 100× on six to seven random fields of view, depending on the coating thickness. Up to 10 random fields were taken for crack length measurements at 200× magnification. The high magnification for crack density measurements was selected in order to detect the fine cracks present in the coating. For the void content analysis, the routine measured only round defects in the weld deposit and excluded linear defects of high aspect ratio. The crack measurement routine was written such that long narrow cracks and voids were measured and excluded round voids that are considered as being porosity. The total crack length for each field was measured and the average crack density for each specimen was calculated in terms of total crack length per unit area.

A JEOL‡ JSM5900LV scanning electron microscope equipped with Oxford energy dispersive x-ray spectroscopy was used for high magnification metallographic examinations. The secondary electron imaging mode was used for all

**Zeiss is a trademark of Carl Zeiss Inc.
†Clemex is a trademark of Clemex Technologies Inc.
‡JEOL is a trademark of Japan Electron Optics Ltd., Tokyo.

examinations. Specimens were viewed with an accelerating voltage ranging from 20 to 25 kV.

3. Results

3.1 Microstructure

3.1.1 Baseline Gas Tungsten Arc Welds. Figure 2 shows HAZ cracking in the baseline gas tungsten arc welds of as-cast Inconel 738 using Inconel 625 filler. As was observed in other research (Ref 3–5), micro-fissures are seen to propagate along grain boundaries into the base material, while the fusion zone was free of cracks.

3.1.2 Metallography of Micro-Weld Deposits. The micro-welded deposits were generally featureless when viewed in the unetched condition by optical and scanning electron microscopy. The deposits appeared uniform and individual droplets were not visible in the majority of test conditions. Etching the polished surfaces with Kalling's no. 2 reagent revealed some droplets in the deposit and a distinctive preferred orientation of fine columnar grains in the order of 3-5 μm in width. The predominant grain alignment was perpendicular to the base material's surface, corresponding to the direction of heat flow during the cooling phase of the micro-weld process. In the coating microstructure, the individual grains were observed to have been formed with several layers of deposition. Figure 3 shows a scanning electron microscope image of the grain structure in an IN625 micro-welded deposit, with some bridging evident. The cast IN738 base material remained free of cracks and did not exhibit a HAZ for all parameters and alloy deposits examined in this study. In general, the micro-welded deposits showed excellent fusion to the base material.

Process parameter selection had a notable effect on the deposit microstructure. Figure 4 and 5 show typical IN738LC micro-welded microstructures for the lowest and highest pulse energy settings, respectively. The volume fraction of porosity and cracking were observed to increase with increasing pulse power setting (current and voltage). Figure 6 and 7 show photomicrographs of IN738LC test specimens micro-welded with Rene 41 and Nimonic 105 filler alloys, respectively.

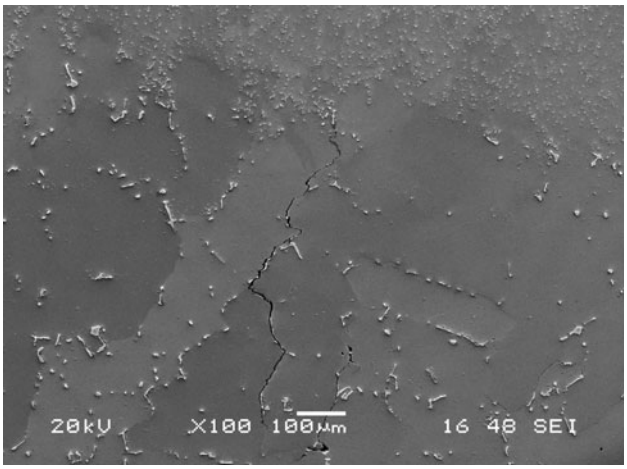

Fig. 2 Intergranular cracks in the heat-affected zone of as-cast Inconel 738 gas tungsten arc welded with Inconel 625 filler. The filler alloy is visible at top portion of the image

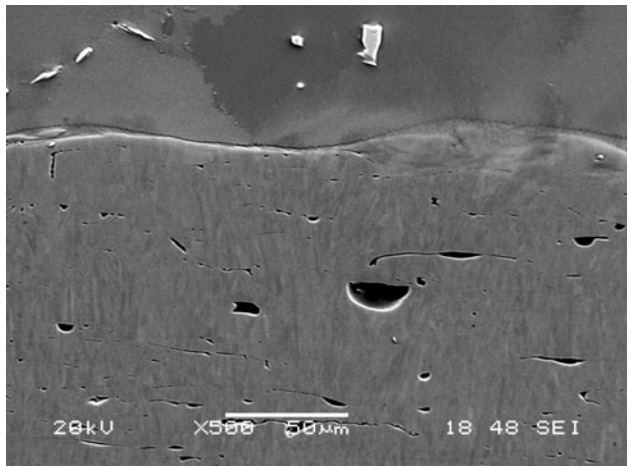

Fig. 3 SEM image of Inconel 625 micro-welded deposit (bottom of image) showing the fine- and oriented-grain structure (5 A, 100 V, 50 μF), swab etched with Kalling's no. 2 reagent

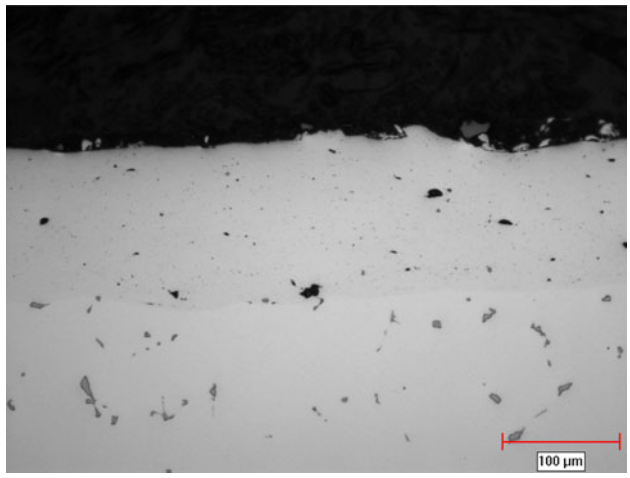

Fig. 4 Inconel 738 micro-weld deposit microstructure displaying a plasma transfer echanism (3 A, 100 V, 20 μF), unetched condition, 200×

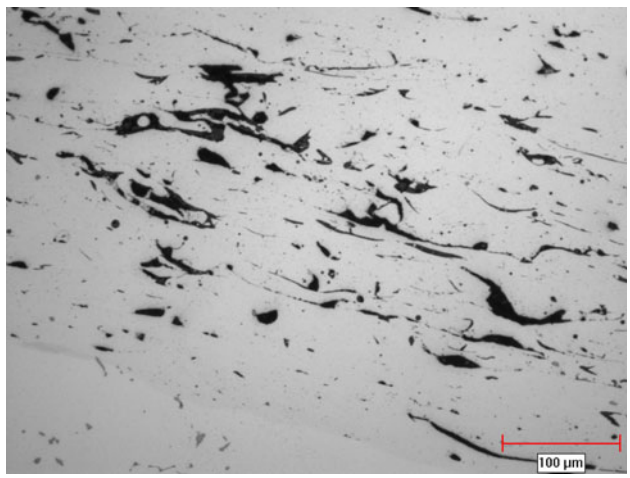

Fig. 5 Inconel 738 micro-weld deposit microstructure displaying plasma, droplet and contact transfer mechanisms (5 A, 200 V, 50 μF), unetched condition, 200×

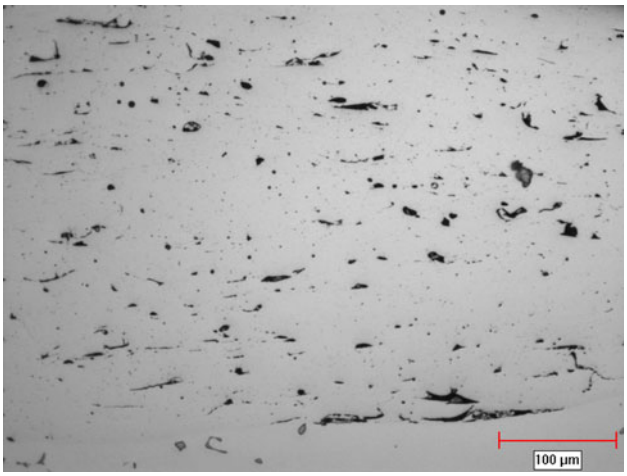

Fig. 6 Microstructure of a Rene 41 micro-welded deposit applied by a plasma transport mechanism (3 A, 200 V, 20 µF), unetched condition, 200×

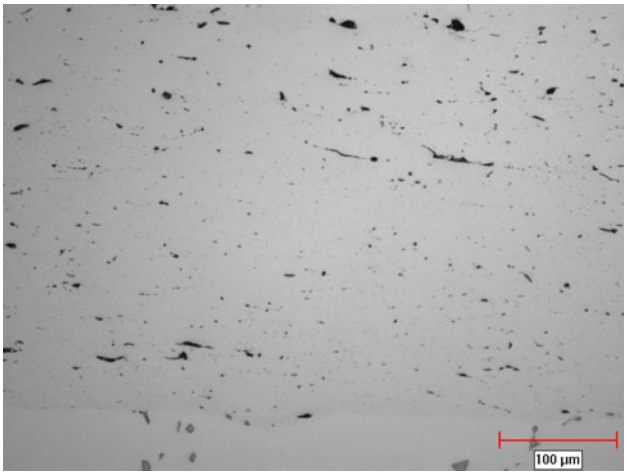

Fig. 7 Microstructure of a Nimonic 105 micro-welded deposit applied by a plasma transport mechanism (5 A, 100 V, 20 µF), unetched condition, 200×

The selection of process parameters was shown to have a significant impact on the resulting microstructure, regardless of the Al + Ti concentration of the filler alloy being welded.

3.2 Statistical Analysis

The results for the responses (deposition rate, void content, and crack density) were analyzed to determine whether the terms (voltage, current, and capacitance) had significant effects. In this study, the terms were considered to have a significant effect on a given response when the p value was <0.1. Two-way interactions, three-way interactions, and curvature were also evaluated for their effect on each response using a threshold p value of 0.1. The interaction terms were capacitance * voltage, capacitance * current, voltage * current, and capacitance * voltage * current. A p value <0.1 for the curvature was considered to have a significant contribution to variation and would therefore not provide an accurate process model. For reference purposes, the percentage of contribution to variation by the main effects, two-way interactions, three-way interactions, and curvature were calculated and are listed in Table 3. SI standard units are used for voltage (V), current (I), and capacitance (F).

3.2.1 Deposition Rate. Experimental results are shown in Appendix 1 for filler alloy IN625. As shown in Table 3, the main effects accounted for 82.3% of the observed variation on deposition rate while the two- and three-way interactions had no significant contributions to the variation. The curvature accounted for 4.7% of the variation. Of the main effects I, V, and F, only the current had a significant effect on deposition rate with a p value of 0.068.

The general model for deposition rate is:

$$\begin{aligned}\text{Deposition rate (g/h)} &= -0.217 + 0.00279 * F + 0.000969 * V + 0.0891 * I \\ &\quad - 2.42\text{E} - 5 * F * V - 0.000545 * F * I \\ &\quad - 0.000270 * V * I + 0.00000443 * F * V * I\end{aligned}$$

With a reduced model for significant terms with p values less than 0.1:

$$\text{Deposition rate (g/h)} = -0.0945 + 0.0528 * I$$

For alloy filler Rene 41, Table 3 and Appendix 2, the main effects for the deposition rate accounted for 77.4% of the

Table 3 Summary of statistical relationships

		Variation contribution of sources, %				
Relationship	**Filler**	**Main effects**	**Two-way interactions**	**Three-way interactions**	**Curvature**	**Comment**
Deposition rate	IN625	82.3	1.6	0.3	4.7	Reduced model structure: main effects
	R41	77.4	7.2	4.1	3.0	Reduced model structure: main effects
	N105	78.0	3.2	0.2	10.7	Reduced model structure: main effects
	IN738	87.5	8.3	1.3	1.3	Reduced model structure: main effects
Void content	IN625	14.3	14.3	4.8	63.6	No possible model, strong curvature with p value of 0.023
	R41	66.5	5.3	0.8	22.6	No possible model, strong curvature with p value of 0.093
	N105	49.1	28.9	5.7	12.4	Reduced model structure: main effects
	IN738	62.6	3.0	0.1	25.8	Reduced model structure: main effects
Crack density	IN625	40.5	6.3	1.6	48.9	No possible model, strong curvature with p value of 0.025
	R41	8.3	35.5	44.5	0.7	No possible model, no significant effects (all p values >0.1)
	N105	65.1	19.1	0.05	14.4	No possible model, strong curvature with p value of 0.040
	IN738	64.5	20.4	11.8	0.007	Reduced model structure: main effects

variation while the two-, three-way interactions, and curvature accounted for 7.2, 4.1, and 3.0%, respectively. The voltage and current factors had significant effects on the deposition rate. The general model for deposition rate is:

$$\begin{aligned}&\text{Deposition rate (g/h)}\\&= 0.00452 - 0.0186 * F - 0.00435 * V - 0.00782 * I\\&\quad + 0.000214 * F * V + 0.00432 * F * I\\&\quad + 0.00145 * V * I - 4.81\text{E} - 5 * F * V * I\end{aligned}$$

With a reduced model for significant terms with p values <0.1:

$$\text{Deposition rate (g/h)} = -0.523 + 0.00220 * V + 0.108 * I$$

The results for Nimonic 105 are shown in Appendix 3 and summarized in Table 3. The main effects for deposition rate accounted for 78.0% of the variation while the two- and three-way interactions accounted for 3.2 and 0.2%, respectively. The curvature had a p value of 0.243 and accounted for 10.7% of the variation. The voltage was the only term that had a significant effect on the deposition rate with a p values of 0.079. The general model for deposition rate is:

$$\begin{aligned}&\text{Deposition rate (g/h)}\\&= -0.230 + 0.00305 * F + 0.00141 * V + 0.0312 * I\\&\quad - 0.0000318 * F * V - 0.000433 * F * I\\&\quad + 0.0000953 * V * I + 0.00000993 * F * V * I\end{aligned}$$

With a reduced model for significant terms with p values <0.10:

$$\text{Deposition rate (g/h)} = -0.0322 + 0.00207 * V$$

Using filler alloy 738, the main effects accounted for 87.5% of the observed variation in deposition rate. The capacitance, voltage, and current terms had significant effects with p values below 0.10. With a p value of 0.322, the curvature in the results accounted for 1.3% of the variation. Refer to Appendix 4 and Table 3 for results. The general model for deposition rate is:

$$\begin{aligned}&\text{Deposition rate (g/h)}\\&= -0.517 + 0.0114 * F + 0.00238 * V + 0.120 * I\\&\quad - 0.000105 * F * V - 0.00326 * F * I\\&\quad - 0.000256 * V * I + 0.0000369 * F * V * I\end{aligned}$$

With a reduced model for significant terms with p values <0.1:

$$\begin{aligned}&\text{Deposition rate (g/h)}\\&= -0.907 + 0.00481 * F + 0.00286 * V + 0.161 * I\end{aligned}$$

3.2.2 Void Content. With filler alloys IN625 and Rene 41, the combination of main effects, two- and three-way interactions, gave low model accuracies while curvature showed significant effects. As a result, meaningful process models for the effect of process parameters on void content could not be generated. Refer to Appendices 1 and 3 and the summary shown in Table 3 for detailed experimental and statistical results.

Using filler alloy Nimonic 105, Table 3 and Appendix 3 the main effects for void content accounted for 49.1% of the variation in results while the two- and three-way interactions accounted for 28.9 and 5.7%, respectively. The curvature in the results, with a p value of 0.129 accounted for 12.4% of the variation. Voltage had a p value of 0.060 and was the only term to have a significant effect on the void content. A general process model for void content is:

$$\begin{aligned}&\text{Void content (vol.\%)}\\&= 0.133 + 0.133 * F + 0.0147 * V + 0.0667 * I\\&\quad - 0.00123 * F * V - 0.0333 * F * I - 0.00167 * V * I\\&\quad + 0.000333 * F * V * I\end{aligned}$$

With a reduced model for significant terms with p values <0.1:

$$\text{Void content (vol.\%)} = 0.593 + 0.0115 * V$$

With filler alloy IN738, (Appendix 4 and Table 3), the main effects for void content accounted for 62.6% of the observed variation. The two-, three-way interactions, and curvature accounted for 3.0, 0.1, and 25.8%, respectively. With a p value of 0.061, current was the only significant term. The general process model for void content is:

$$\begin{aligned}&\text{Void Content (vol.\%)}\\&= -8.23 + 0.0317 * F + 0.0378 * V + 2.7 * I\\&\quad - 0.000367 * F * V - 0.00500 * F * I - 0.00883 * V * I\\&\quad + 0.0000667 * F * V * I\end{aligned}$$

With a reduced model for significant terms with p values <0.1:

$$\text{Void content (vol.\%)} = -2.85 + 1.55 * I$$

3.2.3 Crack Density. For filler alloys IN625, Rene 41, and Nimonic 105, Appendix 1, 2, and 3 and Table 3, the main effects were low and curvature again showed too high values resulting in no models possible.

With IN738 filler deposits, Appendix 4 and Table 3, the main effects for crack density accounted for 64.5% of the variation while the two-, three-way interactions, and curvature accounted for 20.4, 11.8, and 0.007%, respectively. The voltage and current terms had, with p values of 0.076 and 0.039, respectively, had significant effects on the crack density. The general process model for crack density is:

$$\begin{aligned}&\text{Crack density } (\mu\text{m}/\mu\text{m}^2)\\&= -0.0244 + 0.000660 * F + 0.000201 * V + 0.00735 * I\\&\quad - 6.48\text{E} - 6 * F * V - 0.000200 * F * I - 5.32\text{E}\\&\quad - 5 * V * I + 1.97\text{E} - 6 * F * V * I\end{aligned}$$

With a reduced model for significant terms with p values <0.1:

$$\begin{aligned}&\text{Crack density } (\mu\text{m}/\mu\text{m}^2)\\&= -0.0108 + 0.0000378 * V + 0.00271 * I\end{aligned}$$

4. Discussion of Results

The analysis for the factorial design of experiments showed that changing voltage and current has the most significant effect on deposition rate, void content, and crack density of micro-welded deposits. With the exception of one model, changing the capacitance did not have a significant effect on the response.

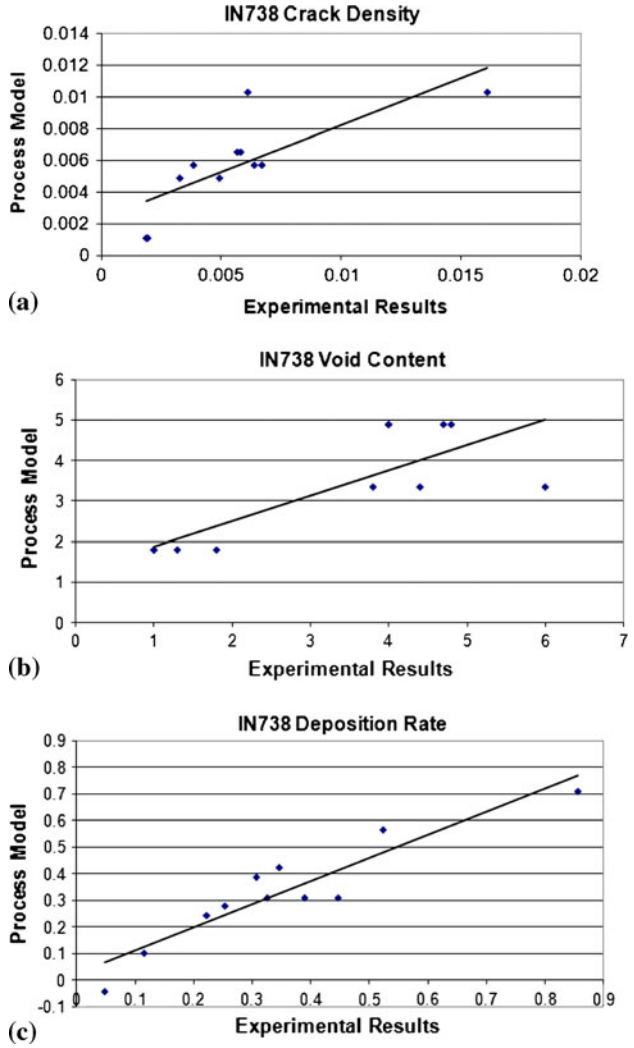

Fig. 8 (a-c) Model predictions vs. actual data for crack density (a), void content (b), and deposition rate (c), for alloy 738

Three examples of the models are plotted in Fig. 8(a-c) for alloy 738, as calculated versus actual values. For crack density, void content, and deposition ratio, the models give correlation coefficient "*r*" values of: 0.77, 0.79, and 0.93, which are significant at the 1% level.

The curvature in the results frequently accounted for a significant portion of the variation. From the process models shown in Tables 4, 5, and 6 general observations are as follows:

- Setting the voltage and current to their maximum values (200 V, 5 A) will increase the deposition rate.
- Setting the voltage and current to their minimum values (100 V, 3 A) will decrease the void content and crack density.
- Varying the capacitance has little to no effect on the deposition rate, void content, and crack density of micro-weld deposits.

Due to the vibration of the electrode during the welding process as the operator traverses the deposit, a range of micro-topographies is observed that can be classified into three types: plasma, droplet, and contact transport mechanism (Ref 11, 14). Previous research by Korobeinik et al. (Ref 14) has shown that

Table 4 Process model coefficients for deposition rate

Model for deposition rate, g/h: $Y = \alpha + \beta F + \gamma V + \delta I - \varepsilon FV - \zeta FI - \eta VI + \theta FVI$

Alloy	α	β	γ	δ	ε	ζ	η	θ
IN625	−0.0945	···	···	0.0528	···	···	···	···
R41	−0.523	···	0.00220	0.108	···	···	···	···
N105	−0.0322	···	0.00207	···	···	···	···	···
IN738	−0.907	0.00481	0.00286	0.161	···	···	···	···

Process models could not be generated when p values >0.10 were obtained

Table 5 Process model coefficients for void content

Model for void content (vol.%): $Y = \alpha + \beta F + \gamma V + \delta I - \varepsilon FV - \zeta FI - \eta VI + \theta FVI$

Alloy	α	β	γ	δ	ε	ζ	η	θ
N105	0.593	···	0.0115	···	···	···	···	···
IN738	−2.85	···	···	1.55	···	···	···	···

Process models could not be generated when p values >0.10 were obtained

Table 6 Process model for crack density

Model for crack density (μm/μm²): $Y = \alpha + \beta F + \gamma V + \delta I - \varepsilon FV - \zeta FI - \eta VI + \theta FVI$

Alloy	α	β	γ	δ	ε	ζ	η	θ
IN738	−0.0108	···	3.78E−5	0.00271	···	···	···	···

Process models could not be generated when p values >0.10 were obtained

the plasma transport topography is generally featureless, while droplets can be readily seen in the microstructure when the droplet transport mechanism operates. Operation of the contact transport mechanism comprises of droplets destroyed during the electrode contact and is seen as bridging within the coating. Figure 9 shows a photomicrograph of an anomalous region where the weld deposit quality was generally poor and displays the three transport mechanisms. The zone of contact transport has the worst properties of the three possible transport mechanisms.

Weld deposits applied by the plasma transport mechanism have the best properties (excellent fusion to the base material, low void, and crack content) and are expected to provide the highest protection against wear and corrosion. However, this level of coating quality can only be achieved at very low deposition rates that may not be practical for the application of this technology. In this study, the process parameters were shown to have a significant effect on the microstructure of micro-welded deposits. The most defect free and metallurgically acceptable deposits were achieved with low voltage and current values, the deposits being relatively featureless and free

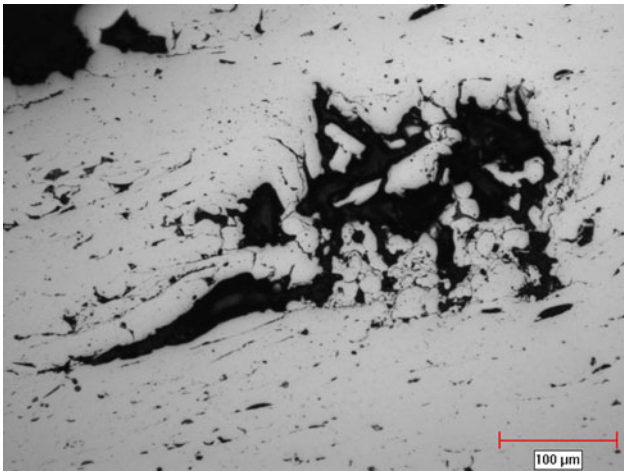

Fig. 9 Microstructure of a Rene 41 micro-welded deposit showing plasma, droplet, and contact transport mechanisms (5 A, 100 V, 20 µF), unetched condition, 200×

of defects. Another observation one can make from the metallographic examination is the absence of a distinct interface between the deposit and base material, confirming that micro-weld deposits are fused to the base material. The use of higher voltage and current values provided higher deposition rates at the expense of increased porosity, cracks, and lack of fusion to the base material. In all but one model, capacitance was shown to have no significant effect on deposition rate, void content, or crack density in the deposits.

Since the conditions for high deposition rate and low porosity and cracking cannot be satisfied simultaneously, the user must tolerate a certain level of defects in the coating. This means that the process parameters that yield the highest deposition rate while maintaining the porosity and cracking within acceptable levels should be selected.

There was no evidence of a HAZ or associated cracking in the cast IN738LC base material for any of weld parameters and filler alloys used in this study. Thakur et al. (Ref 3), Banerjee et al. (Ref 4), and Sidhu et al. (Ref 15) have conclusively shown that the relatively high heat input of the GTA welding process causes HAZ micro-fissuring in IN738LC. Based on the results presented in the present research and (Ref 1), micro-welding is a potentially viable alternative to GTAW for building-up of surfaces on cast high Al + Ti content nickel-base superalloys provided that low deposition rates can be tolerated. The micro-welding process has proven effective in matching the filler to the cast IN738 base material where micro-fissuring in the parent material would otherwise occur by GTAW and result in a reduced component life due the presence of micro-fissures.

5. Conclusions

A micro-welding process was used to evaluate the effect of process parameters on deposition rate, void content, and crack density with filler alloys Inconel 625, Rene 41, Nimonic 105, and Inconel 738. General observations made by the present research are as follows:

- Voltage and current were the most significant process parameters affecting deposition rate, void content, and crack density of micro-welded deposits. The highest deposition rates were obtained with high values for voltage and current (200 V, 5 A). Using low values for voltage and current (100 V, 3 A) reduces void content and crack density. The capacitance did not have a significant effect on the void content and crack density in the deposits.
- Process models were generated relating the effects of capacitance, voltage and current on deposition rate, void content, and crack density. High curvature in the results prohibited the generation of some process models.
- From our previous and present research, micro-welding appears to be a suitable process for repairing Ni-base superalloys with (Al + Ti) contents covering a range of 0.8-6.8 wt.%, especially in alloys extremely susceptible to HAZ micro-fissuring.
- For the micro-weld filler alloys tested in our previous and present research, the cast IN 738LC base material remained free of HAZ micro-cracks. From a purely microstructural analysis, micro-welding appears to be superior to GTAW for the repair of turbine components made from Inconel 738 and potentially for other high strength γ' precipitation strengthened Ni-base superalloys.

Appendices

Appendix 1 Inconel 625 micro-weld deposit

Specimen number	Capacitance, µF	Voltage, V	Current, A	Frequency, Hz floating variable	Deposition rate, g/h	Void content, vol.%	Crack density, µm/µm^2
1	20	100	3	160	0.0671	1.7	0.00122
2	50	100	3	720	0.0690	2.3	0.00222
3	20	200	3	370	0.0612	2.1	0.00241
4	50	200	3	450	0.0304	2.1	0.00227
5	20	100	5	610	0.1872	1.9	0.00205
6	50	100	5	1100	0.1830	2.0	0.00287
7	20	200	5	450	0.1450	2.1	0.00265
8	50	200	5	310	0.1347	2.1	0.00314
9	30	150	4	610	0.0976	1.5	0.00342
10	30	150	4	260	0.1790	1.6	0.00314
11	30	150	4	450	0.1286	1.7	0.00364

Appendix 2 Rene 41 micro-weld deposit

Specimen number	Capacitance, μF	Voltage, V	Current, A	Frequency, Hz floating variable	Deposition rate, g/h	Void content, vol.%	Crack density, μm/μm^2
1	20	100	3	730	0.0063	0.0	0.00995
2	50	100	3	320	0.0450	1.0	0.00426
3	20	200	3	390	0.1452	1.8	0.00594
4	50	200	3	160	0.3931	1.3	0.00879
5	20	100	5	1130	0.2605	4.7	0.00716
6	50	100	5	500	0.2699	4.8	0.00758
7	20	200	5	610	0.4965	4.0	0.00832
8	50	200	5	260	0.4267	4.1	0.00795
9	30	150	4	460	0.1943	3.8	0.00665
10	30	150	4	460	0.3007	5.6	0.00896
11	30	150	4	460	0.0952	4.4	0.00770

Appendix 3 Nimonic 105 micro-weld deposit

Specimen number	Capacitance, μF	Voltage, V	Current, A	Frequency, Hz floating variable	Deposition rate, g/h	Void content, vol.%	Crack density, μm/μm^2
1	20	100	3	730	0.0650	1.5	0.00402
2	50	100	3	320	0.1114	1.8	0.00408
3	20	200	3	380	0.2310	2.0	0.00653
4	50	200	3	160	0.2713	1.6	0.00492
5	20	100	5	1150	0.1688	1.3	0.00322
6	50	100	5	510	0.2488	1.6	0.00498
7	20	200	5	620	0.3936	2.8	0.00847
8	50	200	5	270	0.5271	4.4	0.00891
9	30	150	4	460	0.2491	2.5	0.00668
10	30	150	4	460	0.4125	3.3	0.00761
11	30	150	4	460	0.3872	2.7	0.00734

Appendix 4 Inconel 738 micro-weld deposit

Specimen number	Capacitance, μF	Voltage, V	Current, A	Frequency, Hz floating variable	Deposition rate, g/h	Void content, vol.%	Crack density, μm/μm^2
1	20	100	3	740	0.0479	1.0	0.00189
2	50	100	3	320	0.1151	1.0	0.00195
3	20	200	3	390	0.2216	1.8	0.00494
4	50	200	3	160	0.3068	1.3	0.00329
5	20	100	5	1120	0.2529	4.7	0.00582
6	50	100	5	500	0.3457	4.8	0.00568
7	20	200	5	620	0.5231	4.0	0.00612
8	50	200	5	270	0.8554	4.0	0.01610
9	30	150	4	470	0.4462	3.8	0.00671
10	30	150	4	470	0.3254	6.0	0.00386
11	30	150	4	470	0.3893	4.4	0.00639

References

1. J. Durocher and N.L. Richards, Characterization of the Micro-Welding Process for Repair of Nickel Base Superalloys, *J. Mater. Eng. Perform.*, 2007, **16**(6), p 710–719
2. "Gas Turbine Repair Technology," General Electric Power Systems, Publication # GER-3957B, April 2001
3. A. Thakur, N.L. Richards, and M.C. Chaturvedi, On Crack-Free Welding of Cast Inconel 738, *International Journal for the Joining of Materials*, 2003, **15**(4), p 21–25
4. K. Banerjee, N.L. Richards, and M.C. Chaturvedi, Effect of Filler Alloys on HAZ Cracking in Pre-Weld Heat Treated IN-738 LC GTA Welds, *Metall. Mater. Trans.*, 2005, **36a**, p 1881–1890
5. O.A. Ojo and M.C. Chaturvedi, On the Role of Liquated Gamma Prime Precipitates in Weld Heat Affected Zone Micro-Fissuring of a Nickel-Based Superalloy, *Mater. Sci. Eng.*, 2005, **403**(1–2), p 77–86
6. D.S. Duvall and J.R. Doyle, Repair of Turbine Blades and Vanes, *Gas Turbine Conference and Products Show*, Washington DC, April 8-12, 1973, ASME Report #73-GT-44
7. S. Aoshima, Electro-Spark Processes for Repair and Maintenance of Die-Casting Dies, *Die Cast. Eng.*, Oct 1999, p 64–68
8. W. Gao, Z. Li, and Y. He, High Temperature Oxidation Resistant Coatings Produced by Electro-Spark Deposition, *Mater. Sci. Forum*, 2001, **369–372**(2), p 579–586

9. K.C. Ludema, Electro-Spark Deposition—A Technique for Producing Wear Resistant Coatings, *The International Conference on Wear of Materials*, ASME, Vancouver, BC, Canada, April 14-18, 1985, p 388–395
10. J. Liu, R. Wang, and Y. Qian, The Formation of a Single-Pulse Electrospark Deposition Spot, *Surf. Coat. Technol.*, 2005, **200**, p 2433–2437
11. R.N. Johnson, Electro-Spark Deposition: Principles and Applications, *Society of Vacuum Coaters 45th Annual Technical Conference*, April 2002, p 87–92
12. Y.-J. Xie and M.-C. Wang, Microstructural Morphology of Electro-spark Deposition Layer of a High Gamma Prime Super Alloy, *Surf. Coat. Technol.*, 2006, **201**, p 691–698
13. A. Gregoi and D. Bertaso, Welding & Deposition of Nickel Super Alloys 718, Waspalloy and Single Crystal Alloy CMSX-10, *Weld. World*, 2007, **51**(11/12), p 34–37
14. F. Korobeinik, S.I. Rudyuk, and S.V. Korobeini, Characteristics of the Formation of Micro-Topography, Microstructure and Substructure of the Surface Layer During Electro-Spark Alloying, *Elektr. Obrab. Mater.*, 1989, **1**, p 16–19
15. R.K. Sidhu, N.L. Richards, and M.C. Chaturvedi, Effect of Filler Alloy Composition on Post-Weld Heat Treatment Cracking in GTA Welded Cast Inconel 738LC Superalloy, *Mater. Sci. Technol.*, 2008, **24**(5), p 529–539